

Microscopic aspects of γ -softness in atomic nuclei

Nazira Nazir,¹ S. Jehangir,^{2,*} S.P. Rouoof,² G.H. Bhat,^{3,4,†} J. A. Sheikh,^{1,‡} N. Rather,² and S. Frauendorf^{5,§}

¹*Department of Physics, University of Kashmir, Hazratbal, Srinagar, 190 006, India*

²*Department of Physics, Islamic University of Science and Technology, Jammu and Kashmir, 192 122, India*

³*Department of Physics, S.P. College, Srinagar, Jammu and Kashmir, 190 001, India*

⁴*Cluster University Srinagar, Jammu and Kashmir, Srinagar, Goji Bagh, 190 008, India*

⁵*Department of Physics and Astronomy, University of Notre Dame, Notre Dame, Indiana 46556, USA*

(Dated: September 15, 2022)

The microscopic origin of the γ -softness (fluctuations in the triaxiality parameter γ of the nuclear shape) observed in atomic nuclei is studied in the framework of the triaxial projected shell model approach, which is based on the deformed mean-field picture with multi-quasiparticle configuration space. It is demonstrated that the coupling to quasiparticle excitations drives the system from a γ -rigid to a γ -soft pattern. As an illustrative example for a γ -soft nucleus, a detailed study has been performed for the ^{104}Ru nucleus. The experimental energies and a large sample of measured $E2$ matrix elements available for this nucleus are reproduced quite accurately. The shape invariant analysis of the calculated $E2$ matrix elements elucidates the γ -soft nature of ^{104}Ru .

The central concept of the collective model introduced by Bohr and Mottelson [1] is the shape of the nuclear density distribution, which is parametrized in terms of the multipole fields as in classical electrodynamics. For the interpretation of the low-energy properties, it is sufficient to consider only the quadrupole terms in the multipole expansion. These degrees of freedom are expressed in terms of the β - and γ -shape variables, which measure deviations from the spherical and axial shapes, respectively. The parameters are considered as dynamical variables, the motion of which are determined by the Bohr Hamiltonian. The terminology of "rigid" and "soft" shape is based on its quantum eigenstates with rigid shape signifying small quantum fluctuations around the equilibrium value when the potential has a well defined minimum, and soft shape implies large fluctuations as the potential has a shallow minimum. To delineate these characteristic features from the measured properties as well as their prediction on a microscopic basis has been one of the central research problems in nuclear structure physics [2]. The objective of the present work is to provide a new insight into this problem by addressing the question : how γ -softness originates from the nuclear shell model perspective?

To probe the question, we have chosen ^{104}Ru nucleus as an example because a detailed Coulomb excitation (COULEX) experiment has been performed for this nucleus with the measurement of twenty-eight $E2$ and three $M1$ matrix elements [3] among the low-lying states. Such a large body of matrix elements allows to determine the intrinsic quadrupole moments directly from the experimental data [3]. From the analysis of the shape invariants [4, 5], derived from the set of $E2$ matrix elements, it was deduced [3] that ^{104}Ru is " γ -soft", i.e., the γ -degree of freedom is distributed over a wide range between prolate ($\gamma = 0^\circ$) and oblate ($\gamma = 60^\circ$) shapes.

The adiabatic time-dependent mean-field (ATDMF) approach [6] is the standard method for deriving the parameters of the Bohr Hamiltonian from the fermionic degrees of freedom, which is expounded in the review papers [2, 7]. The

authors of Ref. [3] compared the observed data with a variant of the ATDMF approach [8], which they called the microscopic quadrupole collective Bohr Hamiltonian (QCBH). The method is based on the micro-macro mean-field and Inglis-Belyayev inertia terms (see e.g. Ref. [2]). These calculations reproduced the matrix elements from the COULEX experiment with a good accuracy. In particular, the dispersions of the shape invariants indicated that ^{104}Ru nucleus is γ -soft, which is consistent with the shallow potential of the microscopic Bohr Hamiltonian. The authors of Ref. [9], based on the ATDMF approach with relativistic energy density functional as the mean-field, also reproduced the energies of the ground- and γ -bands in ^{104}Ru quite well.

In this Letter, we interpret the observed data from a microscopic perspective, and demonstrate that experimental energies and the COULEX matrix elements are accurately reproduced in the framework of the triaxial projected shell model (TPSM) approach [12]. In particular, the important features of γ -softness are obtained without considering a collective Hamiltonian, instead they emerge directly by mixing multi-quasiparticle configurations with a fixed mean-field deformation. It was demonstrated in Ref. [11] that TPSM approach reproduces the experimental staggering of the γ -band for a number of nuclei, classifying them as γ -soft or γ -rigid according to staggering criterion. In this work, we demonstrate for the first time that the TPSM reproduces the more direct criterion for γ -softness of large dispersion in the shape invariants deduced from the $E2$ transition matrix elements. It is observed that the dynamics of triaxiality is governed by mixing of a relatively small number of low-lying two-quasiparticle configurations. The method of shape invariants has been used to extract intrinsic quadrupole deformations from large-scale spherical shell model calculations (see Ref. [13] and early work cited therein).

The basic methodology of the TPSM approach is similar to that of the standard spherical shell model with the exception that angular-momentum projected deformed basis is em-

ployed to diagonalize the shell model Hamiltonian [?]. The Hamiltonian consists of monopole pairing, quadrupole pairing, and quadrupole-quadrupole interaction terms within the configuration space of three major oscillator shells ($N = 3, 4, 5$ for neutrons and $N = 2, 3, 4$ for protons) :

$$\hat{H} = \hat{H}_0 - \frac{1}{2}\chi \sum_{\mu} \hat{Q}_{\mu}^{\dagger} \hat{Q}_{\mu} - G_M \hat{P}^{\dagger} \hat{P} - G_Q \sum_{\mu} \hat{P}_{\mu}^{\dagger} \hat{P}_{\mu}, \quad (1)$$

where \hat{H}_0 is the spherical single-particle potential [14]. The pairing parameters are taken from our earlier work [15] with G_M chosen such that the overall observed odd-even mass differences are reproduced for nuclei in this region, and the quadrupole pairing strength G_Q is assumed to be 0.18 times G_M . The QQ-force strength χ is obtained by the self-consistency relation $2\hbar\omega\varepsilon = 3\chi \langle \Phi | \hat{Q}_0 | \Phi \rangle$ [?].

The shell model Hamiltonian of Eq. (1) is diagonalized in the space of angular-momentum projected multi-quasiparticle states. In the present work, the basis is composed of the 0-qp vacuum, the two-quasiproton, the two-quasineutron and the combined four-quasiparticle configurations

$$\begin{aligned} & \hat{P}_{MK}^I | \Phi \rangle, \hat{P}_{MK}^I a_{p_1}^{\dagger} a_{p_2}^{\dagger} | \Phi \rangle, \hat{P}_{MK}^I a_{n_1}^{\dagger} a_{n_2}^{\dagger} | \Phi \rangle, \\ & \hat{P}_{MK}^I a_{p_1}^{\dagger} a_{p_2}^{\dagger} a_{n_1}^{\dagger} a_{n_2}^{\dagger} | \Phi \rangle, \end{aligned} \quad (2)$$

respectively, where " p " labels the quasiproton and " n " the quasineutron states, P_{MK}^I is the standard three-dimensional angular-momentum projection operator [6], and $| \Phi \rangle$ represents the triaxially-deformed quasiparticle vacuum state.

The electromagnetic transition matrix elements are calculated using the electric quadrupole tensor $\mathcal{M}(E2)_{\mu}$ with the effective charge of $1.5e$ for protons and $0.5e$ for neutrons, and the magnetic dipole operator $\mathcal{M}(M1)_{\mu}$ with the spin g factors reduced by a factor of 0.75 [16]. The deformed basis states are generated from a mean-field Nilsson Hamiltonian with fixed deformation parameters $\varepsilon = 0.258$ and $\varepsilon' = 0.150$, which corresponds to a triaxiality parameter of $\gamma = \arctan(\varepsilon'/\varepsilon) = 30.2^{\circ}$. As in our earlier studies [11, 16, 17], these two parameters were adjusted to reproduce the $B(E2, 2_1^+ \rightarrow 0_1^+)$ value [18] and the energy $E(2_2^+)$ of the γ -band of ^{104}Ru . Moreover, the pairing strength was reduced by a factor of 0.5 for the bands built on the excited 0_2^+ and 0_3^+ states.

Fig. 1 compares the TPSM energies with the experimental data and also with the corresponding energies obtained in the QCBH approach. It is evident from the figure that the TPSM reproduces the experimental energies quite well. Fig. 2 displays the staggering parameter

$$S(I) = \frac{[E(I) - E(I-1)] - [E(I-1) - E(I-2)]}{E(2_1^+)} \quad (3)$$

obtained from the corresponding energies of the γ -band. The experimental $S(I)$ depicts the even-I-down pattern of a γ -soft nucleus, which is very well reproduced by the TPSM calculations that include the quasiparticle admixtures. TPSM results with the vacuum configuration only show the odd-I-down pattern of a γ -rigid nucleus. The feature of the γ -softness is,

therefore, generated by the quasiparticle admixtures. The QCBH values indicate γ -softness as well, however, overestimate the amplitude of $S(I)$.

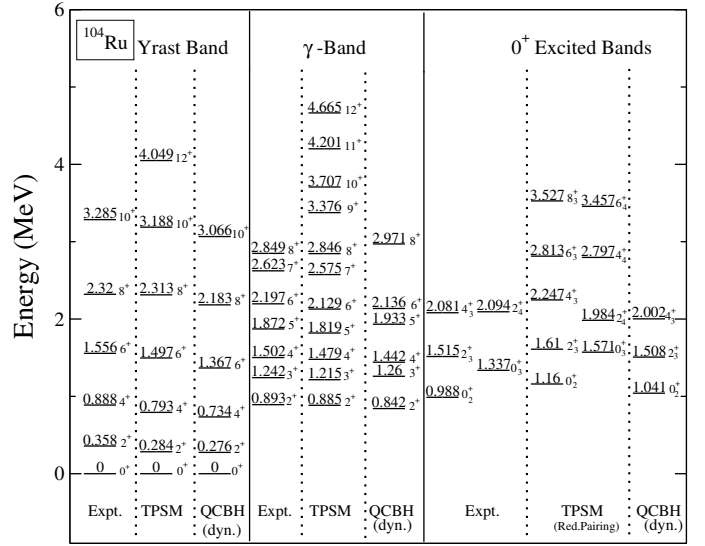


FIG. 1. Comparison of the measured energy levels of ^{104}Ru nucleus with the results of TPSM and QCBH (dyn.) calculations.

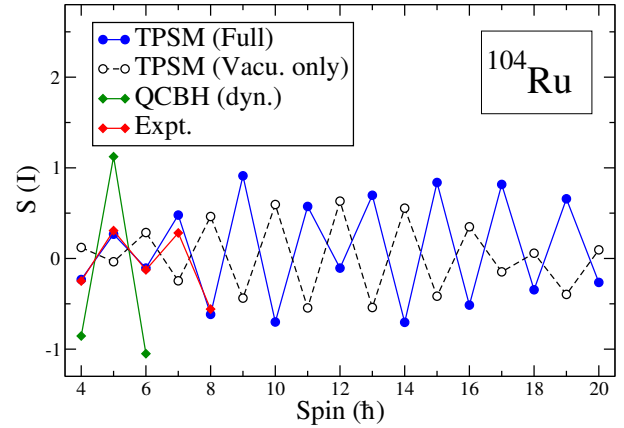


FIG. 2. (Color online) Comparison of the observed (Expt.), QCBH (dyn.) and TPSM (Full) staggering parameter $S(I)$ for the γ -band in ^{104}Ru . The TPSM values without coupling to the quasiparticle excitations are denoted by Vacu. only.

Tables I and II compare the experimental reduced $E2$ matrix elements with the ones calculated using the TPSM wavefunctions. The corresponding values of the QCBH calculations are given in the Tables 1-3 of Ref. [3]. The common signs of the eigenvectors obtained by diagonalization depend on numerical details and do not have physical relevance. The authors of Ref. [3] (Section 6) fixed the signs by choosing the signs of selected non-diagonal matrix elements. We adopted their convention. As can be seen, the matrix elements of the

TABLE I. Comparison of all known experimental reduced $E2$ diagonal, in-band and inter-band matrix elements $\langle I_i || E2 || I_f \rangle$ ($e.b.$), (associated errors in parenthesis) and calculated ones for yrast- and γ -band of ^{104}Ru .

$I_i \rightarrow I_f$	Expt.	TPSM (Full)	TPSM (Vacu.)	$I_i \rightarrow I_f$	Expt.	TPSM (Full)	TPSM (Vacu.)
$2_1 \rightarrow 2_1$	-0.71(11)	-0.817	-0.634	$4_2 \rightarrow 3_1$	± 0.68 (5)	-0.787	-0.597
$4_1 \rightarrow 4_1$	-0.79(15)	-0.906	-0.437	$5_1 \rightarrow 3_1$	1.22(4)	1.184	0.697
$6_1 \rightarrow 6_1$	$-0.70^{(+30)}_{(-20)}$	-0.868	-0.342	$6_2 \rightarrow 4_2$	1.52 (12)	1.521	0.682
$8_1 \rightarrow 8_1$	$-0.6^{(+3)}_{(-3)}$	-0.855	-0.297	$8_2 \rightarrow 6_2$	2.02(4)	2.056	0.747
$2_2 \rightarrow 2_2$	0.62(8)	0.648	0.633	$2_2 \rightarrow 0_1$	-0.156 (2)	-0.141	-0.225
$4_2 \rightarrow 4_2$	-0.58(18)	-0.749	-0.534	$2_2 \rightarrow 2_1$	-0.75(4)	-0.722	-0.612
$6_2 \rightarrow 6_2$	± 1.0 (3)	-1.105	-0.763	$2_2 \rightarrow 4_1$	$\epsilon [-0.1, 0.1]$	-0.090	-0.001
$2_1 \rightarrow 0_1$	0.917 (25)	0.973	0.901	$3_1 \rightarrow 2_1$	0.22(10)	0.254	0.302
$4_1 \rightarrow 2_1$	1.43 (4)	1.591	1.456	$3_1 \rightarrow 4_1$	-0.57	-0.517	-0.559
$6_1 \rightarrow 4_1$	2.04 (8)	2.081	1.830	$4_2 \rightarrow 2_1$	-0.107 (8)	-0.113	-0.054
$8_1 \rightarrow 6_1$	$2.59^{(+24)}_{(-9)}$	2.486	1.902	$4_2 \rightarrow 4_1$	-0.83(5)	-0.840	-0.505
$10_1 \rightarrow 8_1$	2.7 (6)	2.668	1.623	$6_2 \rightarrow 4_1$	$-0.22^{(+6)}_{(-12)}$	-0.230	-0.682
$3_1 \rightarrow 2_2$	-1.22 (10)	-1.241	-0.935	$6_2 \rightarrow 6_1$	> -0.84	-0.947	-0.411
$4_2 \rightarrow 2_2$	1.12(5)	1.095	0.510				

TABLE II. Comparison of all known experimental reduced $E2$ matrix elements $\langle I_i || E2 || I_f \rangle$ ($e.b.$), diagonal, in-band and inter-band values (associated errors in parenthesis) and calculated ones for excited 0^+ bands of ^{104}Ru .

$I_i \rightarrow I_f$	Expt.	TPSM	$I_i \rightarrow I_f$	Expt.	TPSM
$2_3 \rightarrow 0_2$	0.71(4)	0.682	$2_3 \rightarrow 4_1$	-0.370(4)	-0.311
$4_3 \rightarrow 2_3$	0.75(25)	0.613	$2_3 \rightarrow 2_2$	$\pm 0.22^{(+25)}_{(-5)}$	-0.237
$0_2 \rightarrow 2_1$	-0.266(8)	-0.221	$2_3 \rightarrow 4_2$	$0.31^{(+13)}_{(-6)}$	0.221
$0_2 \rightarrow 2_2$	0.08 (3)	0.099	$2_3 \rightarrow 4_4$	$0.53^{(+32)}_{(-14)}$	0.481
$2_3 \rightarrow 0_1$	-0.071(3)	-0.048	$0_3 \rightarrow 2_1$	> -0.1	-0.201
$2_3 \rightarrow 2_1$	± 0.07 (3)	-0.031	$2_3 \rightarrow 2_3$	-0.08($^{11}_{25}$)	-0.631

TABLE III. Comparison of all known experimental reduced $M1$ matrix elements $\langle I_i || M1 || I_f \rangle$ (μ_N), in-band and inter-band values (associated errors in parenthesis) and calculated ones for ^{104}Ru .

$I_i \rightarrow I_f$	Expt.	TPSM	$I_i \rightarrow I_f$	Expt.	TPSM
$2_1 \rightarrow 3_1$	-0.054($^{+9}_{-6}$)	-0.044	$2_1 \rightarrow 2_1$	0.82(10)	0.791
$2_1 \rightarrow 2_2$	< 0.02	-0.038	$4_1 \rightarrow 4_2$	-0.15($^{+3}_{-3}$)	-0.136

two conceptually different approaches are rather similar. The agreement of the TPSM results with the COULEX data is remarkable, because the $E2$ matrix elements provide the most direct information on the statics and dynamics of the collective quadrupole modes. Comparing with the matrix elements Vacu. shows that the quasiparticle admixtures generate the substantial shifts needed for the good agreement with the experiment. Table III presents TPSM reduced $M1$ matrix elements, which also reproduce the known experimental values quite well.

Fig. 3 depicts the quadrupole shape invariants and their dispersions calculated from the reduced $E2$ matrix elements. The pertaining expressions are given in Refs. [3–5]. The invariant $\langle I_n^+ | Q^2 | I_n^+ \rangle$ measures the average intrinsic deformation of a state I_n^+ . The invariant $\langle I_n^+ | \cos 3\delta | I_n^+ \rangle$ contains the

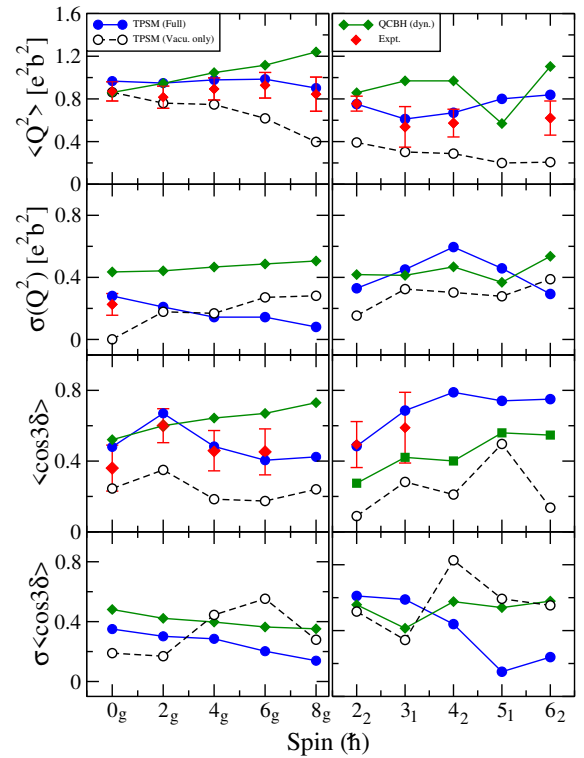


FIG. 3. (Color online) Comparison of the observed (Expt.), QCBH (dyn.) and TPSM shape invariants for the ground-band (left panels) and γ -band (right panels) in ^{104}Ru . The quantities in this figure and in Fig. 5 have been calculated using the code GOSIA [19].

information about the triaxiality of the intrinsic shape, where $\delta = \arctan \langle I_n^+ | \cos 3\delta | I_n^+ \rangle$. The parameters Q and δ can be related to the effective deformation parameters β and γ of the liquid drop model [1]. The relevant formulae for ellipsoidal shape are given in the appendix of Ref. [3]. Evaluating them, we found $\delta < \gamma$ with $|\delta - \gamma| < 2.5^\circ$.

The TPSM value $\langle Q^2 \rangle \approx 1.0(eb)^2$ for the ground-band are nearly constant in agreement with the experimental data. The corresponding effective deformation of $\beta = 0.28$ is the input in the TSPM. The TPSM value of $\langle Q^2 \rangle \sim 0.7$ corresponding to $\beta = 0.27$ indicate a smaller deformation for the γ -band, which is again consistent with the experiment.

For the ground-band, the TPSM values of $\langle \cos 3\delta \rangle$ signify a substantial triaxiality with preference for prolate shape. The value of 0.6 corresponds to $\delta = 18^\circ$ or $\gamma = 20^\circ$. For $I = 2$, the experimental data shows a shift toward prolate shape, which is seen in the TPSM values as well. The QCBH values are similar, showing a steady shift toward the prolate shape with increasing I . The TPSM dispersion $\sigma \langle \cos 3\delta \rangle \sim 0.3$ signifies large fluctuations of the triaxiality parameter with 70% of the distribution within the range $9^\circ < \delta < 24^\circ$. Hence, the TSPM shape invariants indicate that ^{104}Ru is γ -soft in accordance with the staggering parameter $S(I)$ of Fig. 2. The QCBH dispersion of $\sigma \langle \cos 3\delta \rangle \sim 0.4$ corresponds to a distribution with 70% in the larger range $0^\circ < \delta < 26^\circ$. The

QCBH values seem to overestimate the γ -softness, which is consistent with the QCBH values for $S(I)$ being larger than the TSPM and the experimental values.

For the γ -band, the TSPM values of $\langle \cos 3\delta \rangle$ for $I = 2, 3$ and 4 indicate a shift toward prolate shape, which is in accordance with the experimental values. This shift is also seen in the QCBH calculation, which predicts a larger $\delta \sim 24^\circ$ as compared to $\delta \sim 18^\circ$ of TSPM. The dispersions are similar to the ones in the ground-band.

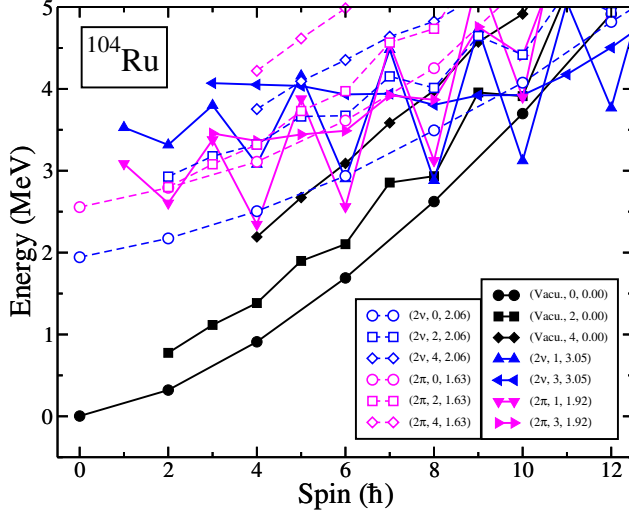


FIG. 4. (Color online) TSPM projected energies before band mixing. The bands are labelled by three quantities : quasiparticle character, K -quantum number and energy of the two-quasiparticle state. For instance, $(2\nu, 1, 3.05)$ designates the $K = 1$ state projected from the $h_{11/2}$ two-quasineutron configuration with the energy of 3.05 MeV. The $K = 0, 2, 4$ states projected from the quasiparticle vacuum configuration are labelled with Vacu. The four-quasiparticle states lie above 5 MeV.

In order to probe the microscopic origin of the appearance of γ -soft characteristics, the energies of the angular momentum projected quasiparticle configurations are depicted in Fig. 4. The $K = 0, 2, 4, \dots$ states, projected from the quasiparticle vacuum configuration, have an increasing content of the angular momentum oriented along the long-axis with the smallest moment of inertia. For $K = 0$, there are only even- I states. When the TSPM Hamiltonian is diagonalized with vacuum configuration only, it mostly couples the $K = 0$ with the $K = 2$ states. The coupling pushes up the even- I states of the γ -band above the mean energy of the adjacent $K = 2$ states with odd I , which are not shifted because they do not have a partner in the ground-band. This results in the odd- I low pattern of the staggering parameter $S(I)$.

In the TSPM diagonalization, the most important quasiparticle admixtures to the γ -band are the $K = 1$ state projected from the $h_{11/2}$ two-quasineutron configuration and the $K = 1, 3$ states, projected from the $g_{9/2}$ two-quasiproton configuration. Their admixtures increase with I and is about 20% for

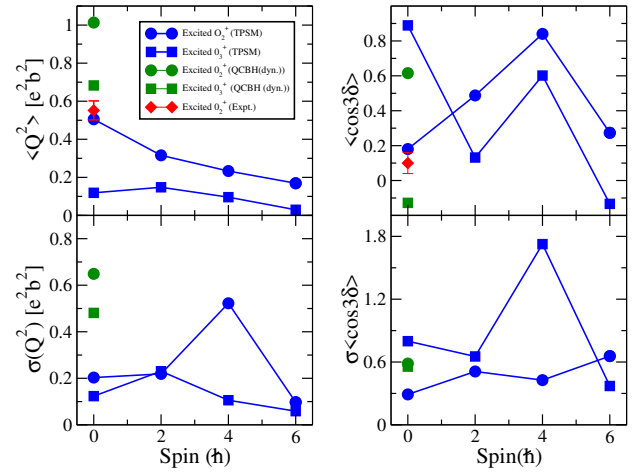


FIG. 5. (Color online) Comparison of the observed (Expt.), QCBH (dyn.) and TSPM shape invariants for the excited 0^+ bands in ^{104}Ru .

the $I = 7$ state. As noted from Fig. 4, these quasiparticle band structures show a pronounced even- I low staggering. The coupling pushes the states with even I further down than the states with odd I , and the coupling is strong enough to reverse the staggering pattern of the γ -band into the even- I low pattern of a γ -soft nucleus. The high- j orbitals $h_{11/2}$ and $g_{9/2}$ have large quadrupole moments, and a moderate admixture of these states modifies the $E2$ matrix elements such that the pattern of a γ -soft nucleus emerges from the γ -rigid pattern of the vacuum configuration only. The superposition of configurations with different triaxiality increases the shape fluctuations as seen in Fig. 3.

A further indication for γ -softness is the appearance of a $\Delta I = 2$ band built on an excited 0_2^+ state which is connected by collective $E2$ transitions with the γ band. In terms of the collective Bohr Hamiltonian, it represents a pulsation of the triaxial surface that carries no angular momentum (see Fig. 6 of the review [2]). The limiting cases are the $K = 0$ double γ vibration of the axially symmetric potential and the 0_2^+ state of the γ -independent potential, where it represents the oscillation between prolate and oblate shapes through a triaxial path. The COULEX experiment observed 0_2^+ and 0_3^+ states of this type [3]. As seen in Fig. 1 and Table II, the TSPM calculations account well for the experimental data. For the 0_2^+ state, the shape invariant $\langle \cos 3\delta \rangle$ in Fig. 5 indicates strong triaxiality of $\delta = 26^\circ$, which decreases toward the prolate value of zero with I . For the 0_3^+ state, weak triaxiality is noted that increases to the maximal value with I . The dispersions indicate large fluctuations in δ . The 0_2^+ state contains a 60% component of the $K = 0$ two $h_{11/2}$ quasineutron configuration $(2\nu, 0, 2.06)$ in Fig. 4), which decreases to 20% for the 6_3^+ state by admixing many small components. The 0_3^+ state contains a 95% component of the $K = 0$ two $g_{9/2}$ quasiproton configuration $(2\pi, 0, 1.63)$ in Fig. 4), which decreases to 40% for the 6_4^+ state by admixing many small components.

The dominating two-quasiparticle character of the $0_{2,3}^+$ states justifies the reduction of the pairing strength in the TPMSM calculation, which lie too high in the excitation energy with full strength (see Fig. 4). The QCBH calculations [3] also point to a change of the pair correlation. The dynamic variant of QCBH, which takes into account the coupling to the pairing field provides the right excitation energy, whereas the static variant without the coupling gives too large energies [3].

In summary, we have shown that TPMSM approach reproduces the extended set of collective $E2$ matrix elements measured in the COULEX experiment with a remarkable accuracy. The shape invariant quantities deduced from these matrix elements capture the features of a γ -soft nucleus with the mean value of the triaxiality parameter of $\delta \sim 20^\circ$, and fluctuations within the range $0^\circ < \delta < 26^\circ$. The important inference drawn from the present analysis is that admixtures of quasiparticle states into the collective vacuum configuration can transform the pattern of the energies and $E2$ matrix elements from γ -rigid to that of γ -soft character. A detailed shape invariant analysis of twenty-two nuclei, the energy staggering analysis of which have been performed in Ref. [11], shall be presented in a detailed publication separately. Finally, it is evident that the spherical shell model calculation with a sufficiently large basis set should capture the discussed collective features [13]. However, the small number of quasiparticle configurations within the present deformed shell model approach provides another perspective on the nature of γ -softness in atomic nuclei: It represents the superposition of a few configurations with different triaxiality.

ACKNOWLEDGEMENTS

The authors acknowledge the Science and Engineering Research Board (SERB), Department of Science and Technology (Govt. of India) for providing financial assistance under the Project No.CRG/2019/004960, and for the award of INSPIRE fellowship to one of the author (NN). We are also indebted to Drs. L. Próchniak, P. J. Napiorkowski and J. Srebrny for providing some unpublished results, and for their assistance in running the GOSIA code.

* sheikhahmad.phy@gmail.com

† gwahr.bhat@gmail.com

‡ sjphysics@gmail.com

§ sfraugend@nd.edu

- [1] A. Bohr and B. R. Mottelson, *Nuclear Structure* (World Scientific Publishing Company, 1998), <https://www.worldscientific.com/doi/pdf/10.1142/3530>, URL <https://www.worldscientific.com/doi/abs/10.1142/3530>.
- [2] S. Frauendorf, *International Journal of Modern Physics E* **24**, 1541001 (2015), URL <https://doi.org/10.1142/S0218301315410013>.
- [3] J. Srebrny, T. Czosnyka, C. Droste, S. Rohoziński, L. Próchniak, K. Zajac, K. Pomorski, D. Cline, C. Wu, A. Bäcklin, et al., *Nuclear Physics A* **766**, 25 (2006), ISSN 0375-9474, URL <https://www.sciencedirect.com/science/article/pii/S0375947405012029>.
- [4] D. Cline, *Annual Review of Nuclear and Particle Science* **36**, 683 (1986), URL <https://doi.org/10.1146/annurev.ns.36.120186.003343>.
- [5] K. Kumar, *Phys. Rev. Lett.* **28**, 249 (1972), URL <https://link.aps.org/doi/10.1103/PhysRevLett.28.249>.
- [6] P. Ring and P. Schuck, *The Nuclear Many-Body Problem* (Springer Berlin Heidelberg, 1980), URL <https://link.springer.com/book/9783540212065>.
- [7] T. Nikšić, D. Vretenar, and P. Ring, *Progress in Particle and Nuclear Physics* **66**, 519 (2011), ISSN 0146-6410, URL <https://www.sciencedirect.com/science/article/pii/S0146641011000561>.
- [8] K. Zajac, L. Próchniak, K. Pomorski, S. Rohoziński, and J. Srebrny, *Nuclear Physics A* **653**, 71 (1999), ISSN 0375-9474, URL <https://www.sciencedirect.com/science/article/pii/S037594749900161X>.
- [9] Z. Shi and Z. P. Li, *Phys. Rev. C* **97**, 034329 (2018), URL <https://link.aps.org/doi/10.1103/PhysRevC.97.034329>.
- [10] J. A. Sheikh and K. Hara, *Phys. Rev. Lett.* **82**, 3968 (1999), URL <https://link.aps.org/doi/10.1103/PhysRevLett.82.3968>.
- [11] S. Jehangir, G. H. Bhat, J. A. Sheikh, S. Frauendorf, W. Li, R. Palit, and N. Rather, *Eur. Phys. J. A* **57**, 308 (2021), URL <https://doi.org/10.1140/epja/s10050-021-00620-7>.
- [12] J. A. Sheikh and K. Hara, *Phys. Rev. Lett.* **82**, 3968 (1999), URL <https://link.aps.org/doi/10.1103/PhysRevLett.82.3968>.
- [13] A. Poves F. Novacki and Y. Alhassid, *Phys. Rev. C* **101**, 054307 (2020), URL <https://doi.org/10.1142/S0218301395000250>.
- [14] S. G. Nilsson, C. F. Tsang, A. Sobiczewski, Z. Szymański, S. Wycech, C. Gustafson, I.-L. Lamm, P. Möller, and B. Nilsson, *Nucl. Phys. A* **131**, 1 (1969), ISSN 0375-9474, URL <https://www.sciencedirect.com/science/article/pii/0375947469908094>.
- [15] J. A. Sheikh, G. H. Bhat, W. A. Dar, S. Jehangir, and P. A. Ganai, *Phys. Scr.* **91**, 063015 (2016), URL <https://doi.org/10.1088/0031-8949/91/6/063015>.
- [16] S. Jehangir, G. H. Bhat, J. A. Sheikh, R. Palit, and P. A. Ganai, *Nucl. Phys. A* **968**, 48 (2017), ISSN 0375-9474, URL <https://www.sciencedirect.com/science/article/pii/S0375947417303408>.
- [17] S. Jehangir, G. H. Bhat, N. Rather, J. A. Sheikh, and R. Palit, *Phys. Rev. C* **104**, 044322 (2021), URL <https://link.aps.org/doi/10.1103/PhysRevC.104.044322>.
- [18] S. Raman, C. Nestor, and P. Tikkanen, *Atomic Data and Nuclear Data Tables* **78**, 1 (2001), ISSN 0092-640X, URL <https://www.sciencedirect.com/science/article/pii/S0092640X01908587>.
- [19] D. Cline, T. Czosnyka, A. Hayes, P. Napiorkowski, N. Warr, and C. Wu, *Gosia User Manual For Simulation And Analysis Of Coulomb Excitation Experiments*, Rochester NY US (2012), URL http://www.pas.rochester.edu/~cline/Gosia/Gosia_Manual_20120510.pdf.